# DEVELOPMENT OF FABRICATION TECHNIQUES FOR MESOPOROUS AND MESOSTRUCTURED MATERIALS

by

Bryce Alexander Turner

A thesis submitted to the faculty of
The University of Utah
in partial fulfillment of the requirements of the degree

Master of Science

Department of Chemistry

The University of Utah

August 2015

The University of Utah Graduate School

# STATEMENT OF THESIS APPROVAL

The thesis of Bryce Alexander Turner

has been approved by the following supervisory committee members:

| | | |
|---|---|---|
| Michael H. Bartl | , Chair | 5/26/2015 Date Approved |
| Scott L. Anderson | , Member | 5/27/2015 Date Approved |
| Thanh L. Truong | , Member | 5/27/2015 Date Approved |

and by Cynthia J. Burrows , Chair of

the Department of Chemistry

and by David B. Kieda, Dean of The Graduate School.

## ABSTRACT

Materials that have feature sizes on the mesoscale present unique properties based on diffusion and chemical reactions. Despite the breadth of work done in this area, there is little work done connecting biological mesostructures and the well-developed inorganic mesoporous materials. This thesis presents work done on mesostructured and mesoporous materials to connect biological mesostructures to the field of inorganic mesoporous materials. Specifically, we have developed novel methods for making self-assembled biological-inorganic mesoporous composites, densified mesoporous solids, and investigated tunability of mesostructured biological emulsions (cubosomes).

Cubosomes were investigated for tunability of the lattice parameter via addition of a designer peptide and was characterized by cryogenic transmission electron microscopy and small-angle x-ray scattering, which revealed a swelling of the lattice parameter and the appearance of a hexagonal phase at low peptide concentrations. Self-assembled biological-inorganic composite materials was shown to possess order on the mesoscale when observed by transmission electron microscopy and were loaded with Rhodamine B. Fluorescence studies revealed successful loading of the dye and changes in the salt or acid concentration unloaded the dye. SBA-type silica was densified while maintaining mesoporosity using spark plasma sintering and proof of principle were done to

illustrate how these materials could be chemically modified into semiconductors relevant to energy applications.

“Chemistry is just a word
We use to describe what occurs
When subtle changes in your minds
Make energy from common lives”
*Magic Word,* Damien Abraham, 2008

## TABLE OF CONTENTS

## LIST OF TABLES

## LIST OF FIGURES

## LIST OF ABBREVIATIONS

BET- Brunauer-Emmett-Teller theory

Cryo-TEM- Cryogenic Transmission Electron Microscopy

HR-TEM- High Resolution Transmission Electron Microscopy

LLC- Lyotropic Liquid Crystal

MCM-41- Mesoporous Silica with Cubic Symmetry (Mobile Corporation)

MO- Monoolein

MOF- Metal-Organic Framework

OA- Oleic Acid

PBS- Phosphate Buffered Saline

PL- Photoluminescence

TEM- Transmission Electron Microscopy

TEOS- Tetraethyl Orthosilicate

SAXS- Small-Angle X-ray Scattering

SBA-15- Mesoporous Silica with Hexagonal Symmetry (UC Sante Barbara)

SBA-16- Mesoporous Silica with Cubic Symmetry (UC Santa Barbara)

SPS- Spark Plasma Sintering

WALP- Designer Peptide of one alpha helix, sequence given in chapter 2.

XPS- X-ray Photoelectron Spectroscopy

XRD- X-ray Diffraction

# CHAPTER 1

## INTRODUCTION

Nanoscale materials have been of great interest to researchers in recent years due to their striking and unique size- and shape-dependent properties. These vary from electronic and optical properties[1] which take advantage of quantum effects to properties based on diffusion[2] and chemical reactions[3] on the nanoscale.

Nanoporous materials belong to the latter group and are defined as any material featuring pores with a nanometer-sized diameter. They can have feature sizes anywhere from the tenths of nanometers up to hundreds of nanometers and be composed of organic or inorganic components. While several different definitions can be found in the literature, IUPAC defines microporous as having pore sizes under two nanometers, mesoporous having pores between two and 50 nanometers, and macroporous having pores larger than 50 nanometers.[4] The IUPAC definition will be used through this thesis.

Porous materials can be applied to a myriad of applications. Typical microporous materials are metal-oxide frameworks and zeolite structures, which are used for ion-exchange[5], molecular sieves[6], and insulation materials[7]. Macroporous materials have attracted attention for applications in photonic band

gap materials and other metamaterials.[8] Of the three types of porous materials, mesoporous materials have attracted the most interest from researchers in recent years. This is due to the ease and variety of synthesis techniques[9,10] and range of possible chemical functionalities.[11,12] These have led to a dazzlingly vast array of applications including catalysis[13], separation[14,15], sorption[16,17,18], sensing[19,20], drug delivery[21,22], optics[23,24], and optoelectronics.[25]

Most of the nanostructured porous frameworks, or ‘symmetries’, of these nanoscale materials are still impossible to fabricate through lithographic techniques, the technique most common for macroporous material, but they can be formed successfully through supramolecular assembly combined with sol-gel based techniques which either template a polymeric liquid crystal type structure or cooperatively assemble with the structure-directing units. Both of these methods take advantage of the amphiphilic nature of surfactants, which generally consist of a hydrophilic head group of varying chemical functionalities and a hydrophobic carbon tail.

While both methods use a structure directing species, they differ in the timing and method of incorporating silica. For templating-based techniques, the surfactants form into a mesostructure with water and a metal-oxide is subsequently condensed within the hydrophilic domains of the structure via a sol-gel process. This technique usually involves ionic surfactants to create electrostatic interactions between the charged head group and the silica precursors prior to silica condensation. The first supramolecular assembly method was developed by researchers at Mobile Corporation and created MCM-

type materials consisting of ordered alumina-silica while attempting to create more effective zeolite catalysts.[26] Shortly after, Galen Stucky's group at the University of California, Santa Barbara, showed how non-ionic surfactants can be used in dilute acid solutions with a silica precursor such as tetraethyl orthosilicate (TEOS) to form ordered mesoporous materials, termed SBA-type materials.[9] This method was quickly adopted by many researchers due to the ease of synthesis, thermal stability of the material, and larger pore sizes than MCM-type silica.

Since the development of silica mesoporous materials, the field has greatly expanded into mesoporous materials based on other metal-oxides,[27] chalcogenides,[28,29] metals,[30] and various forms of carbon.[31] There have been a wide range of techniques developed for synthesizing powders and thin-films[32], but there is yet a definitive method for creating large bulk solids. Traditional densification methods are incapable of maintaining the mesostructure of the material during the densification process due to pore collapse. Densification would allow for creating tailored shapes for porous membranes, battery components, and catalytic materials. This thesis will present work done on how a relatively new technique of spark plasma sintering (SPS) can be applied to mesoporous silica and successfully densify the material while maintaining the ordered mesostructure.

The second focus of this thesis will be on the development of robust synthetic methods for hybrid lipid-silica mesostructured composites. In the last 25 years, researchers in biomedical fields and food sciences have increasingly focused on developing and investigating routes for using lipid structures for drug

delivery vectors[33], emulsifiers[34], and hosts for crystallization of membrane proteins.[35] This was based almost exclusively on one particular lipid, 1-oleoyl-*rac*-glycerol or monoolein (MO), a lipid composed of an eighteen carbon chain with a *cis* double bond at carbon eight and a glycerol head group. From small-angle x-ray scattering experiments this lipid had been known since the 1960's to produce organic liquid crystal-based mesostructures.[36,37]

Since then, a breathtaking array of theoretical work has been done to explain the topologically complex symmetries formed. Additionally, efforts had been undertaken to link the geometric complexities to the cubic membrane systems found in many organisms but little work had been done on potential applications of these structures.[38,39] Later, Landh and Larsson reported the discovery of emulsified forms of the lyotropic liquid crystals: nanoparticles with the same symmetry as these important liquid crystal organic mesostructures. In 1996, they were also the first to file a patent on ordered lipid systems in which the term 'cubosome' was first used.[40] Since then, researchers have developed numerous additional methods for fabricating cubosomes, and applications of the system range from drug delivery to electrotemplating of lipid liquid crystals.[41,42,43]

Despite these initial successes and enormous potential of cubosomes, no work has been done so far to connect the lipid mesostructures with inorganic condensation chemistry. Such a combination would enable stabilization of the 'fluid' cubosome mesostructured symmetries through conversation into hybrid organic-inorganic or purely inorganic frameworks, with interesting applications in drug delivery and bio-imaging. This thesis presents the first steps in this direction

by connecting lipid mesophases with the broader field of ‘conventional’ mesoporous materials. Several methods for producing hybrid lipid-silica composites based on a new co-assembly method have been developed. We also investigated structural features of dilute cubosomes systems first developed by Spicer *et al.* and studied their interaction with silica-based sol-gel chemistry.[44,45] We will present the developed synthesis method, provide detailed structural characterization results, and conclude with a discussion of potential applications of these new materials.

## 1.1 References

1. Qi, X.L.; Zhang, S.C. Topological Insulators and Supercondutors. *Rev. Mod. Phys.* **2011,** *83* (4), 1057

2. Notomi, M. Manipulating Light With Strongly Modulated Photonic Crystals *Rep. Prog. Phys.* **2010,** *73* (9), 096501

3. Perego, C.; Millini, R. Porous Materials in Catalysis: Challenges for Mesoporous Materials. *Chem. Soc. Rev.* **2013,** *42*, 3956-3976

4. McCusker, I.B.; Liebau, F.; Engelhardt, G. Nomenclature of Structural and Compositional Characteristics of Ordered Microporous and Mesoporous Materials with Inorganic Hosts *Pure Appl. Chem.* **2001,** *73* (2). 381-394

5. Townsend, R.P. Ion Exchange in Zeolites: Some Recent Developments on Theory and Practice *Pure Appl. Chem.* **1986,** *58* (10), 1359-1368

6. Lok, B.M.; Messina, C.A.; Patton, R.L.; Gajek, R.T.; Cannan, T.R.; Flanigan, E.M. Siicoaluminophsophate Molecular Sieves: Another New Class of Microporous Crystalline Inorganic Solids *J. Am. Chem. Soc.* **1984,** *106* (20), 6092-6093

7. Kratel, G.; Stohr, G.; Schreiner, F., Shaped Microporous Thermal Insulation Body with Sheating and Process for Making Same. U.S. Patent 4636416 A. Jan. 13, 1987
.
8. Joannopoulos, J.D.; Villeneuve, P.R.; Fan, S. Photonic Crystals: Putting a New Twist on Light *Nature* **1997,** *386,* 143—149

9. Zhao, D.; Huo, Q.; Feng, J.; Chmelka, B.F.; Stucky, G.D. Nonionic Triblock and Star Diblock Copolymer and Oligomeric Surfactant Synthesis of Highly Ordered, Hydrothermally Stable Mesoporous Silica Structures. *J. Am. Chem. Soc.* **1998,** *120*, 6024-6036

10. Rahmat, N.; Abdullah, A.Z.; Mohamed, A.R. A Review: Mesoporous Santa Barba Amorphous-15 Types, Synthesis and Its' Applications Towards Biorefinery Production. *Am. J. Appl. Sci.* **2010,** *7* (10), 1579-1586

11. Yang, P.; Gai, S.; Lin, J. Functionalized Mesoporous Silica Materials for Controlled Drug Delivery *Chem Soc. Rev.* **2012,** *41,* 3679-3698

12. Xu, P.; Yu, H.; Li, X. Functionalized Mesoporous Silica for Microgravimetric Sensing of Chemical Vapor *Anal. Chem.* **2011,** *83* (9), 3448-3454

13. Taguchi, A.; Schuth, F. Ordered Mesoporous Materials in Catalysis. *Microporous Mesoporous Mater.* **2005,** *77* (1), 1-45

14. Zhao, J.; Gao, F.; Fu, Y.; Jin, W.; Yang, P.; Zhao, D. Biomolecule Seperation Using Large Pore Mesoporous SBA-15 as a Substrate in High Performance Liquid Chromatography *Chem. Commn.* **2002,** *7,* 752-753

15. Yu, C.; Fan, J.; Tian, B.; Zhao, D. Morphology Development of Mesoporous Materials: a Colloidal Phase Seperation Mechanism *Chem. Mater.* **2004,** *16* (5), 889-898

16. Beck, J.S.; Vartuli, J.C.; Roth, W.J.; Leonowicz, M.E.; Kreege, C.T.; Schmitt, K.D.; Chu, C. T-W.; Olson, D.H.; Sheppard, E.W.; McCullen, S.B.; Higgins, J.B.; Schlenker, J.L. A New Family of Mesoporous Sieves Prepared with Liquid Crystal Templates *J. Am. Chem Soc.* **1992,** *114,* 10834-10843

17. Fan, J.; Yu, C.; Gao, F.; Lei, J.; Tian, B.; Wang, L.; Luo, Q.; Tu, B.; Zhou, W.; Zhao, D. Cubic Mesoporous Silica with Large Controllable Entrance Sizes and Advnced Adsorption Properties *Angew. Chem.* **2003,** *115* (27), 3254-3258

18. Pahalagedara, L.R.; Poyraz, A.S.; Song, W.; Kuo, C.H.; Pahalagedara, M.D.; Meng, Y.T.; Sulb, S.L. Low Temperature Desulfurization of $H_2S$: High Sorption Capacities by Mesoporous Cobalt Oxide via Increased $H_2S$ Diffusion *Chem. Mater.* **2014,** *26* (22), 6613-6621

19. Melde, B.J., Johnson, B.J., Charles, P.T. Mesoporous Silicate Materials in Sensing. *Sensors* **2008,** *8*, 5202-5228

20. Li, L.; He, S.; Liu, M.; Zhang, C.; Chen, W. Three-Dimensional Mesoporous Graphene Aerogel-Supported $SnO_2$ Nanocrystals for High-Performance $NO_2$ Gas Sensing at Low Temperature *Anal. Chem.* **2015,** *87* (3), 1638-1645

21. Argyo, C; Weiss, V.; Brauchle, C.; Bein, T. Multifunctional Mesoporous Silica Nanoparticles as a Universal Platform for Drug Delivery. *Chem Mater.* **2014,** *26* (1), 435-451

22. Chen, X.; Cheng, X.; Soeriyadi, A.H.; Sagnella, S.M.; Lu, X.; Scott, J.A.; Lowe, S.B.; Kavallaris, M.; Gooding, J.J. Stimuli-Responsive Functionalized Mesoporous Silica Nanoparticles for Drug Release in Response to Various Biological Stimuli. *Biomater. Sci.* **2014,** *2,* 121-130

23. Bartl, M.H.; Puls, S.P.; Tang, J.; Lichtenegger, H.C.; Stucky, G.D. Cubic Mesoporous Frameworks with a Mixed Semiconductor Nanocrystalline Wall Structure and Enhanced Sensitivity to Visible Light. *Angew. Chem. Int. Ed.* **2004**, *43*, 3037-3040.

24. Bartl, M.H.; Boettcher, S.W.; Hu, E.L.; Stucky, G.D. Dye-Activated Hybrid Organic/Inorganic Mesostructured Titania Waveguides. *J. Am. Chem. Soc.* **2004**, *126*, 10826-10827.

25. Crossland, E.J.W.; Noel, N.; Sivaram, M.; Leijtens, T.; Alexander-Weber, J.A.; Snaith, H.J. Mesoporous $TiO_2$ Single Crystals Delivering Enhanced Mobility and Optoelectronic Device Performance. *Nature* **2013,** *495*, 215-220

26. Kresge, C.T.; Leonowicz, M.E.; Roth, W.J.; Vartuli, J.C.; Beck, J.S. Ordered Mesoporous Molecular Sieves Synthesized by a Liquid-Crystal Template Mechanism. *Nature* **1992,** *359*, 710-712

27. Bastakoti, B.P.; Ishihara, S.; Leo, S.Y.; Ariga, K.; Wu, K.C.W.; Yamauchi, Y. Polymeric Micelle Assembly for Preparation of Large-Sized Mesoporous Metal Oxides with Various Compositions *Langmuir* **2014,** *30* (2), 651-659

28. Yonemoto, B.T.; Hutchings, G.S.; Jiao, F. A General Synthetic Approach for Ordered Mesopoorous Metal Sulfides *J. Am. Chem. Soc.* **2014,** *136* (25), 8895-8898

29. Makovicky, E. Micro- ad Mesoporous Sulfide and Selenide Structures *Rev. Mineral. Geochem.* **2005,** *57* (1), 403-434

30. Ataee-Esfahani, H.; Imura, M.; Yamauchi, Y. All-Metal Mesoporous Nanocolloids: Solution-Phase Synthesis of Core-Shell Pd@Pt Nanoparticles with a Designed Concave Surface *Angew. Chem., Int. Ed.* **2013,** *52* (51), 13611-13615

31. Hu, Y.S.; Adelhelm, P.; Smaarsly, B.M.; Hore, S.; Antonietti, M; Maier, J. Synthesis of Hierachically Porous Ordered Carbon Monoliths with Highly Ordered Microstructure and Their Application in Rechargeable Lithium Batteries with High-Rate Capabilities. *Adv. Funct. Mater.* **2007,** *17* (12), 1873-1878

32. Zhao, D.; Yang, P.; Margolese, D.I.; Chmelka, B.F.; Stucky, G.D. Synthesis of Continuous Mesoporous Silica Thin-Films with Three-Dimensional Accessible Pore Structure. *Chem. Commun.* **1998,** *22*, 2499-2500

33. Negrini, R.; Mezzenga, R. pH-Responsive Lyotropic Liquid Crystals for Controlled Drug Delivery *Langmuir* **2011,** *27* (9), 5296-5303

34. Pichot, R., Spyropoulos, F., Norton, I.T. Mixed-Emulsifier Stabilised Emulsions: Invesitfation of the Effect of Monoolein and Hydrophilic Silica Particle Mixtures on the Stability Against Coalescence *Jour. Colloid Interface Sci.* **2009,** *329* (2), 284-291

35. Caffrey, M. Membrane Protein Crystallization *J. Struct. Biol.* **2003,** *142* (1), 108-132

36. Delacroix, H.; Nicolas, G.; Gulik-Krzywicki, T. 3-Dimensional Organization of Cubic Membranes: Study of Endoplamis Reticulum Paracrystals in Photosomes. *Biol. Cell* **1998,** *90* (3), 288

37. Deng, Y.; Mieczkowski, M. Three-Dimensional Periodic Cubic Membrane Structure in the Mitochondria of Amoebae *Chaos carolinensis*. *Protoplasma* **1998**, *203* (1-2), 16-25

38. Anderson, D.M.; Gruner, S.M.; Leibler, S. Geometrical Aspects of the Frustration in the Cubic Phase of Lyotropic Liquid Crystals. *Proc. Natl. Acad. Sci.* **1988,** *85*, 5364-5368

39. Qui, H.; Caffrey, M. The Phase Diagram of Monoolein/Water System: Metastability and Equilibrium Aspects. *Biomaterials* **2000,** *21* (3), 223-234

40. Landh, T.; Larsson, K., Particles, Method of Preparing Said Particles and Uses Thereof. U.S. Patent 5,531,925 A, Jul. 2, 1996.

41. Lakshmi, N.M.; Yalavarthi, P.R.; Vadlamudi, H.C.; Thanniru, J.; Yaga, G.K.H. Cubosomes as Targeted Drug Delivery Systems – A Biopharmaceutical Approach. *Curr. Drug Discovery Technol.***2014,** *11* (3), 181-188

42. Razumas, V.; Kanapleniene, J.; Nylander, T.; Engstrom, S.; Larsson, K. Electrochemical Biosensors for Glucose, Lactate, Urea, and Creatinine Based Enzymes Entrapped in a Cubic Liquid Crystalline Phase *Anal. Chim. Acta* **1994,** *289* (2), 155-162

43. Braun, P.V.; Osenar, P.; Tohver, V.; Kennedy, S.B.; Stupp, S.I. Nanostructure Templating of Inorganic Solids with Organic Lyotropic Liquid Crystals *J. Am. Chem. Soc.* **1999,** *121,* 7302-7309

44. Spicer, P.T. Progress in Liquid Crystalline Dispersions: Cubosomes. *Curr. Opin. Colloid Interface Sci.* **2005,** *10*, 274-279

45. Kaehr, B.; Townson, J.L.; Kalinich, R.M.; Awad, Y.H.; Swartzentruber, B.S.; Dunphy, D.R.; Brinker, C.J. Cellular Complexity Captured in Durable Silica Biocomposite *Proc. Natl. Acad. Sci. U.S.A.* **2012,** *109* (43), 17336-17341

# CHAPTER 2

# MESOSTRUCTURED LIPID MATERIALS

## 2.1 Introduction

Lipids are broadly defined as amphiphilic molecules consisting of a hydrophobic carbon “tail” and a hydrophilic “head”. The tail can consist of a variety of lengths and may include *cis* or *trans* double bonds. The head can be composed of a wide variation of chemical functional groups. The size ratio of the head group to the tail will vary the structure that is formed when lipids self-assemble. This is defined as the packing parameter of the lipid, which can be expressed mathematically as

$$p = \frac{v}{a \cdot l} \tag{1}$$

where *p* is the packing parameter, *v* is the volume of the hydrocarbon tail, *a* is the area of the headgroup, and *l* is the length of the hydrocarbon chain. The packing parameter can be used to determine the curvature of the lipid structure. If $p > 1$, then the structure will have negative curvature, if $p < 1$ the structure will have

positive curvature and $p$ = 1 will result in no curvature (see Figure 2.1). Monoolein has a positive curvature (i.e. curves towards water) and will produce structures with constant positive curvature.

MO and other lipid mesostructures may be formed either in a lyotropic liquid crystal (LLC) phase where the only components are water and the lipid or they may be dispersed with a small amount of block copolymer. The dispersions maintain the liquid crystal structures in form of nanoparticles (~100-500 nm in size with ~10 nm lattice parameters, Figure 2.2). These lipid nanoparticles are termed cubosomes or hexosomes depending on whether the symmetry of the ordered lipid structure is cubic or hexagonal, respectively.[1,2] Many researchers have investigated how the mesostructural ordering of monoolein may be affected by additional compounds including hydrophobic molecules[3], designer peptides[4], and additional lipid components.[5] These have exclusively looked at the bulk phase system while cubosomes and hexosomes have generally only been looked at from an application viewpoint. We have performed structural studies on cubosomes and hexosomes, specifically looking at the effect of a designer peptide on the formation, mesostructural ordering, and stability of the lipid nanoparticles.

There are a several synthesis methods for cubosomes.[6,7] The most common produces a monolith structure with water and lipid and then disperses the monolith into an aqueous environment.[6] An alternative method uses molten lipid and a small amount of block copolymer to emulsify with hydration and sonication in a self-assembly approach.[7] The latter method gives a polydisperse

sample, but is interesting due to the high water content (up to 98% by weight) of the formed cubosomes. Since one of the goals of the thesis is to study how peptide additions can affect the assembly and stability of mesostructured lipid nanoparticles, the latter method was used due to the ease of incorporating additional molecules into the assembly process.

**2.2 Methods**

Cubosomes were assembled by a modified method from Spicer.[7] Briefly, monoolein (purchased from Nu-Chek Prep, used as received), a designer peptide termed WALP19 with an amino-acid sequences of GWWLALALALALALALWWA (synthesized at Utah Core Facilities), and Pluronic® F127, a triblock copolymer with a nominal structure of poly(ethylene oxide)-b-poly(propylene oxide)-b-poly(ethylene oxide), $PEO_{101}PPO_{56}PEO_{101}$ (donated from BASF) were mixed at a composition of 92% w/w lipid/peptide and 8% w/w Pluronic® F127, dried under nitrogen, and placed under vacuum for a minimum of an hour. After the sample was heated to a molten state, water (18 MΩ minimum resistivity) was added to give a final composition of 98% water and the solution was sonicated at room temperature for 60 minutes and stored at room temperature.

Cubosomes were characterized by small angle x-ray scattering (SAXS) and cryogenic transmission electron microscopy (cryo-TEM). SAXS was performed at the Cornell High-Energy Synchrotron Source (CHESS) at beam line D1. Samples were analyzed in a 1.5 mm diameter special glass capillary tube (purchased from Charles Supper Inc.) loaded into a capillary holder with a

temperature controller and placed 13 meters from the x-ray source at 10 keV with a MedOptics CCD detector 564 mm from the sample. Scattering diffractograms were analyzed in Fit2D and Origin software. Cryo-TEM was performed on a FEI Technai 12 microscope. Samples were prepared on 300 mesh lacey carbon grids (purchased from Ted-Pella Inc.) by placing 1.5-3 μL of specimen onto the grid and rapidly plunging into liquid ethane. Grids were viewed in the TEM microscope at 120 keV accelerating voltage.

**2.3 Results and Discussion**

Cryo-TEM results are consistent with a cubosome or hexosome type structure (Figure 2.3). This finding is also supported by SAXS studies, which show a scattering pattern consistent with cubic lipid structures (Figure 2.4). In addition, SAXS data indicate that the ordered structure is strongly affected by the presence of the WALP peptide. While a small amount of peptide breaks the expected cubic symmetry into either a hexagonal or sponge phase, higher peptide concentrations regain the cubic symmetry with a swollen lattice parameter (Table 2.1). The results clearly indicate a strong effect due to the addition of hydrophobic peptides. The variety of symmetries seen with changing peptide concentration indicates a shifting of the phase diagram from that of the bulk phase. The appearance of the sponge phase is particularly intriguing and may represent an intermediate phase between hexagonal and cubic phases.

Perhaps most interestingly, at a concentration of 0.01 mol% WALP peptide a hexagonal symmetry with remarkable thermal stability is formed. While the other samples formed ordered symmetries only within a narrow temperature

range of a few degrees Celsius, the hexagonal symmetry at 0.01 mol% WALP concentration was remarkably stable within a temperature range of 50 °C. Moreover, the ordered structure was maintained for 6 hours at 70 °C (Figure 2.5). To the best of our knowledge, such a wide thermal stability is yet unreported for any lipid nanoparticle.

It is difficult to say exactly what gives rise to the extreme stability of the hexagonal phase. Although hexagonal phases can account for a large thermal range of certain materials,[8] it accounts for a relatively small proportion of the monoolein phase diagram when compared to the cubic phase.[9] However, the conventional phase diagram is unable to accurately inform the behavior of cubosomes and hexosomes, as most phase diagrams do not report water content relevant to our samples. Additionally, assembly conditions of nanoparticles are considerably different from a bulk phase as they are formed in isolated hydrophobic pockets. In short, the monoolein-water phase diagram can be used to guide behavior but cannot provide a direct comparison.

It is possible that the higher thermal stability is a result of the curvature of the system. Several groups have developed geometric models[10,11] that map the Helfrich free energy as a function of curvature. The hexagonal phase has a lower interfacial energy and can more easily adapt to thermal fluctuations by minor distortions in micellar packing. Conversely, the cubic phase only has a small thermal region that it can adjust before incurring too great a free energy cost and undergoing a phase transition. While this may account for the observed behavior, repeat experiments and computational modeling are required for confirmation

and deeper understanding into this behavior. The recent work done on both modeling the facet structure[12] and phase behavior of the membrane during protein crystallization[13] give an excellent starting point for the development of computational models of how peptide addition affects the phase behavior of lipid amphiphiles.

## 2.4 Conclusions

We have demonstrated how WALP peptides can be included into MO cubosome systems with high water contents. The phase behavior of the cubosome system is dramatically affected by the inclusion of the peptide, creating hexagonal systems and sponge phase particles. While there is yet a complete picture of the energetic effects of WALP on cubosome systems, the work presented in this thesis represents the first experimental steps demonstrating the difference between binary cubic phases of monoolein and the nanoparticle form. We have experimentally shown the strong influence of peptide addition to cubosome and hexosome type structures and identified a hexagonal organic material with a unique unreported thermal stability.

## 2.5 References

1. Spicer, P. Cubosome Processing: Industrial Nanoparticle Technology Development *Chem. Eng. Res. Des.* **2005,** *83* (11), 1283-1286

2. Neto, C.; Aloisi, G.; Baglioni, P. Imaging Soft Matter with the Atomic Force Microscopy: Cubosomes and Hexosomes *J. Phys. Chem B.* **1999,** *103* (19), 3896-3899

3. Murgia, S.; Bonacchi, S.; Falchi, A.M>; Lampis, S.; Lippolis, V.; Meli, V.; Monduzzi, M.; Prodi, L.; Schmidt, J.; Taimon, Y.; Caltagirone, C. Drug-Loaded Fluorescent Cubosomes: Versatile Nanoparticles for Potential Theranostic Applications *Langmuir* **2013,** *29* (22), 6673-6679

4. Siegel, D.P.; Cherezov, V.; Greathouse, D.V.; Koeppe II, R.E.; Killan, J.A.; Caffrey, M. Transmembrane Helices Stabilize Inverted Cubic Phases in a Biphasic Length-Dependent Manner: Implications for Protein-Induced Membrane Fusion. *Biophys. J.* **2006,** *90* (1), 200-211

5. Nakano, M.; Teshigawara, T.; Sugita, A.; Leesajakul, W.; Tanigushi, A.; Kamo, T.; Matsuoka, H.; Handa, T. Dispersions of Liquid Crystalline Phases of the Monoolein/Oleic Acid/Pluronic F127 System *Langmuir* **2002,** *18* (24), 9283-9288

6. Landh, T.; Larsson, K., Particles, Method of Preparing Said Particles and Uses Thereof. U.S. Patent 5,531,925 A, Jul. 2, 1996.

7. Spicer, P.T. Progress in Liquid Crystalline Dispersions: Cubosomes. *Curr. Opin. Colloid Interface Sci.* **2005,** *10*, 274-279

8. Barauskas, J.; Landh, T. Phase Behavior of the Phytantriol/Water System *Langmuir* **2003,** *19* (23), 9562-9565

9. Qui, H.; Caffrey, M. The Phase Diagram of Monoolein/Water System: Metastability and Equilibrium Aspects. *Biomaterials* **2000,** *21* (3), 223-234

10. Anderson, D.M.; Gruner, S.M.; Leibler, S. Geometrical Aspects of the Frustration in the Cubic Phase of Lyotropic Liquid Crystals. *Proc. Natl. Acad. Sci.* **1988,** *85*, 5364-5368

11. Shearman, G.C.;Khoo, B.J.; Motherwell, M.L.; Brakke, K.A.; Ces, O.; Conn, C.E.; Seddon, J.M.; Templer, R.H. Calculations of and Evidence for Chain Packing Stress in Inverse Lyotropic Bicontinuous Cubic Phase. *Langmuir* **2007,** *23*, 7276-7285

12. Latypova, L.; Gozdz, W.T.; Pieranski, P. Facets of Lyotropic Liquid Crystals. *Langmuir* **2014,** *30* (2), 4884-95

13. Le, T.C.; Conn, C.E.; Burden, F.R.; Winkler, D.A. Computational Modeling and Prediction of the Complex Time-Dependent Phase Behavior of Lyotropic Liquid Crystals under *in Meso* Crystallization Conditions. *Crys. Growth Des.* **2013,** *13*, 1267-1276

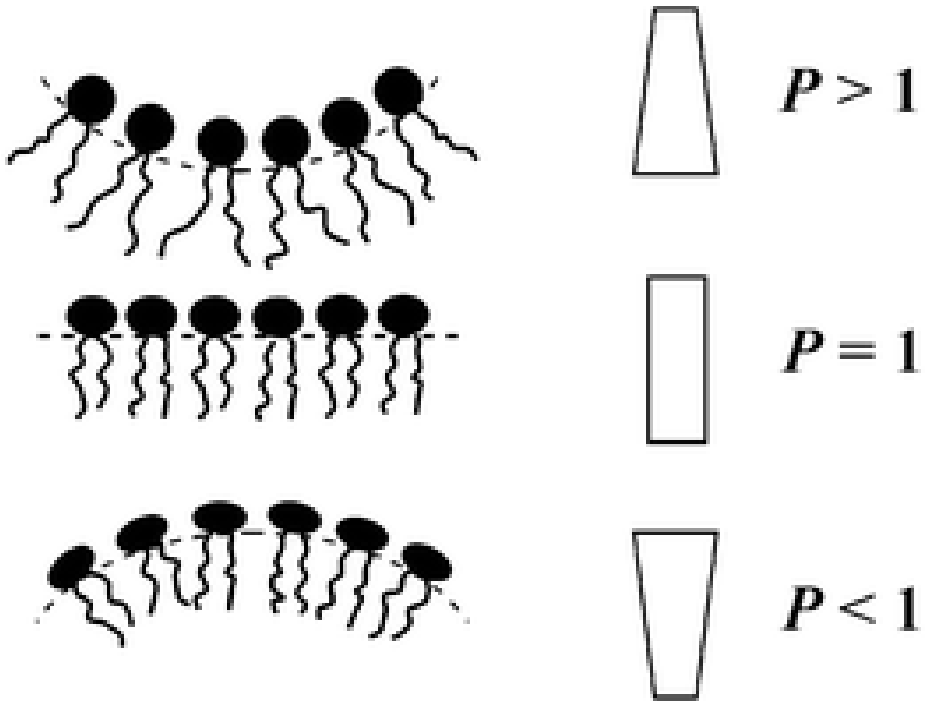


Figure 2.1 Cartoon showing the curvature of ambiphiles in relation to the packing parameter *p*. Reproduced from Winter, R. *et al. Soft Matt.* **2009,** *5,*3157-3173 with permission of The Royal Society of Chemistry.

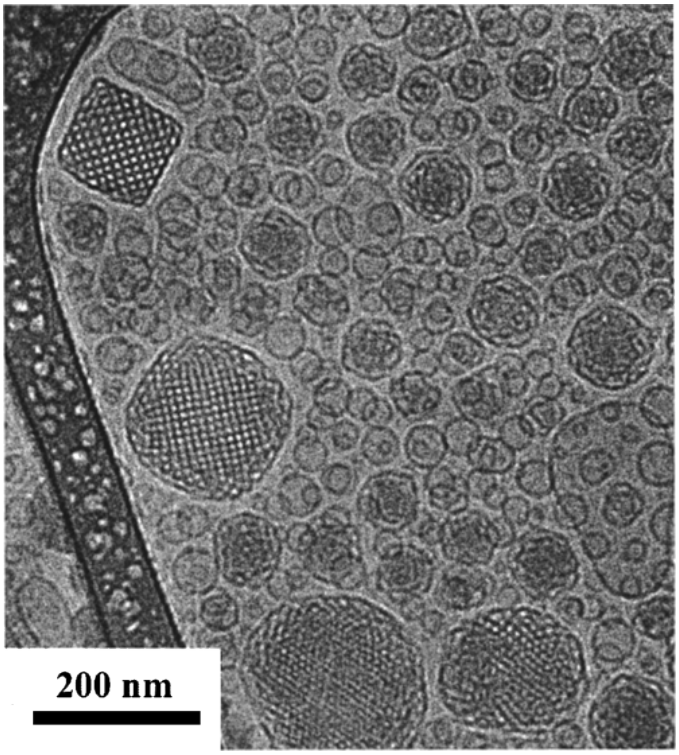


Figure 2.2 Cryo-TEM micrograph of cubosome particles in a polydisperse sample showing cubic particle and vesicles. Reprinted with permission from Spicer. P.T.; Hayden, K.L. Novel Process for Producing Cubic Liquid Crystalline Nanoparticles (Cubosomes) *Langmuir* **2001,** *17* (19), 5748-5756. 

Table 2.1 Calculated symmetries of the lipid microemulsions from SAXS

| Mol% WALP | Symmetry | a (nm) |
|---|---|---|
| 0 | Pn3m/Hexagonal/Lamellar | 9.1 ± 0.5 |
| 0.01% | Hexagonal | 6.97 ± 0.05 |
| 0.05% | Sponge | N/A |
| 0.1% | Sponge | N/A |
| 0.2% | Sponge | N/A |
| 0.3% | N/A | N/A |
| 0.4% | Pn3m | 11.3 ±0.6 |
| 0.5% | Pn3m | 11.9 ±0.9 |

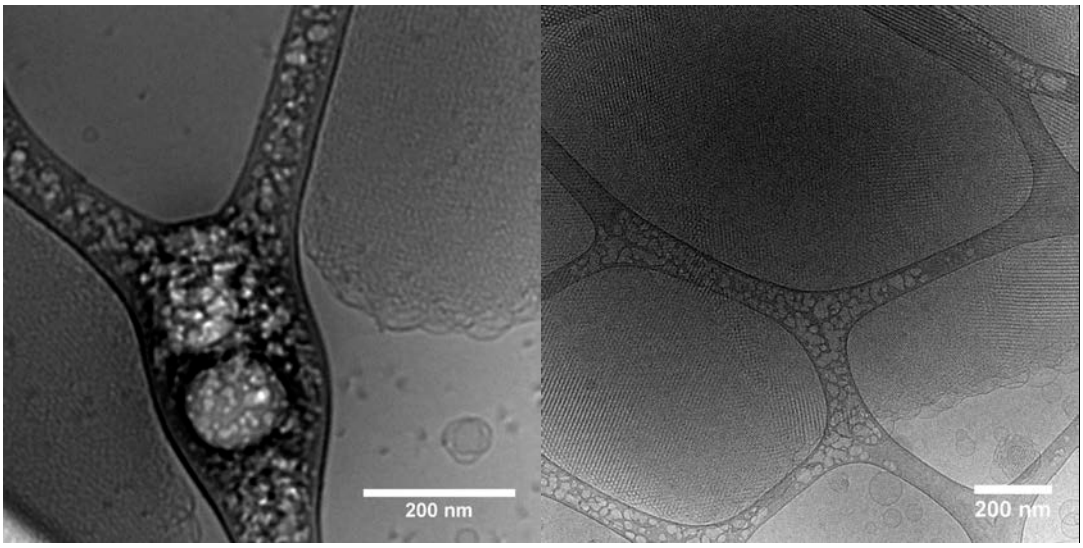


Figure 2.3 Cryo-TEM micrograph of the cubosome and hexosome structures. The image on the left shows two cubosomes against the lacey carbon support (damaged from the electron beam) while the image on the right shows a large aggregate of hexosomes frozen above the carbon support grid.

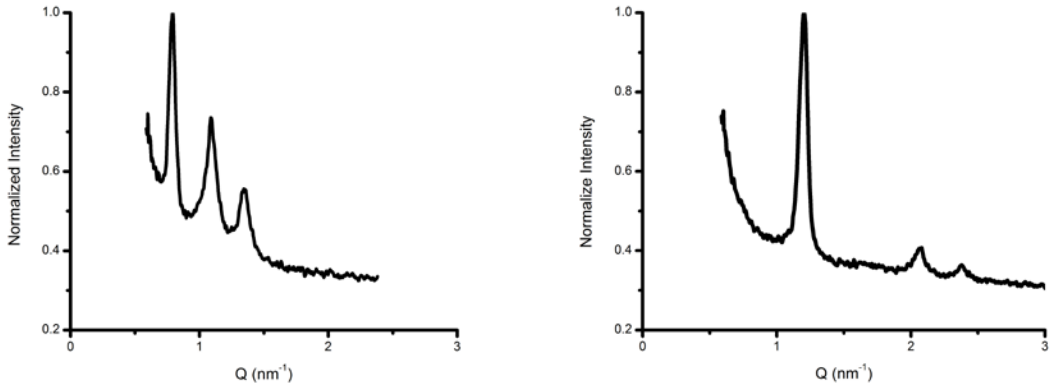


Figure 2.4 Typical SAXS diffractograms for cubosomes (left) and hexosomes (right). The ratio of peaks to the first and strongest peak is used to properly determine the symmetry, where 1:√2:√3 is *Pn3m* and the ratio of 1:√3:√4 is *p6mm*.

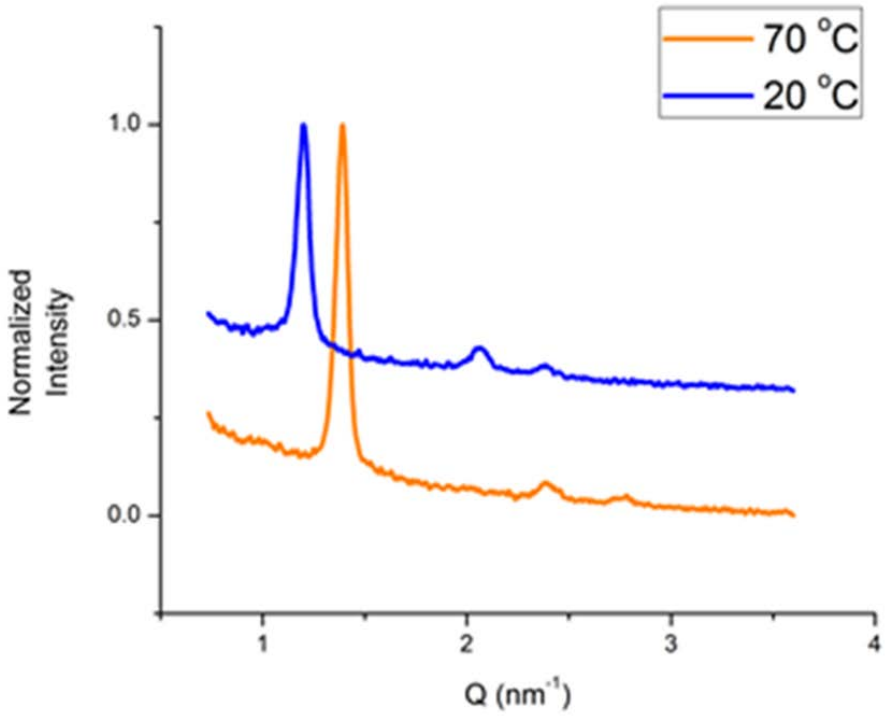


Figure 2.5 SAXS diffractogram showing the thermal stability of the hexosome. The shrinking of the lattice was reversible and the structure was able to withstand high temperature treatment at 70 °C for up to six hours.

# CHAPTER 3

# BIOLOGICAL MESOSTRUCTURED COMPOSITES

## 3.1 Introduction

Composites are defined as any material consisting of two components with different properties. Mesoporous and mesostructured composites have been successfully developed by numerous groups but are generally tailored to a specific metamaterial or application.[1,2,3] In the thesis, the term “mesostructured” will be used for materials in which the structure-directing species remain an integral part of the final material, whereas materials in which the structure-directing species were removed will be termed “mesoporous”.

Use of mesoporous materials for drug delivery and biomedical applications has historically been limited to surface functionalization and loading of silica nanoparticles with a drug solution.[4,5] Part of this thesis research focused on combining bio-compatible components with sol-gel based methods to fabricate self-assembled composite materials[6,7] that can be used to enhance the drug delivery capabilities of previous cubosome structures.[8,9] The inorganic portion of the composite will constitute a protective layer and provide structural stability for *in vivo* use, while the lipid component will be able to load hydrophobic materials.

### 3.2 Methods

Composite cubosome structures were prepared by melting monoolein (MO, purchased from Nu-Check Prep 99.99%) or oleic acid (OA, purchased from Sigma-Aldrich, 90%) with block copolymer Pluronic® F127 at a composition of 92% w/w lipid and 8% Pluronic® F127 until molten and then adding a tetraethyl orthosilicate (TEOS) solution (either prehydrolyzed or mixed directly prior to addition) of between 1-3% w/v TEOS (Sigma-Aldrich) in 1 mM HCl (Sigma-Aldrich) for a final composition of 98 % w/w TEOS solution and sonicating for 60 minutes at room temperature. Samples were then either loaded with a dilute solution of Rhodamine B at 4 °C for seven days, then subsequently washed with water, or calcined at 500 °C for 3 hours with a ramp rate of 1°C/min.

Composite lyotropic liquid crystals (LLC) were made by mixing MO or OA with a 3 % TEOS solution in 1 mM HCl and subsequently performing 10-20 cycles of freezing on dry ice and thawing at 40 °C. These samples were then calcined as described above.

Samples were characterized by TEM, XRD, as well as photoluminescence spectroscopy and microscopy. Samples for TEM imaging were prepared by depositing the composite onto 300 mesh copper grids with either continuous or lacey carbon/formvar cover layers. Samples were observed under 120 keV acceleration voltage on a JEOL JEM-1400 microscope. X-ray diffraction was collected on dried powder samples on a Bruker D8 Advance diffractometer using Cu K$\alpha$ radiation. Photoluminescence spectroscopy was performed on a home-built optical setup (measurement performed by Carlos Burga) using the 514 nm line of an argon ion laser as excitation source. The emission was guided into a

spectrometer, dispersed by a 150 groove/mm grating and recorded by a charge-coupled device (CCD) detector. Photoluminescence microscopy was performed on a modified Nikon Eclipse ME600 optical microscope using an argon ion laser (514 nm line) as excitation. The photoluminescence image was passed through a 550 nm long-pass filter and recorded with a Diagnostic Instruments SPOT Insight 4.0 MP color mosaic CCD camera.

### 3.3 Results and Discussion

Composite silica cubosomes and LLC structures were successfully synthesized, as verified by TEM imaging (Figure 3.1). These results clearly illustrate that it is possible to assemble and stabilize highly ordered silica-lipid hybrid composites with a cubic mesostructured framework. In addition, an intriguing assembly detail is revealed: When the composite is made with MO, there was little to no ordering observed; however, using OA a high amount of cubic ordering was obtained.

This observed preference for OA in self-assembled composite structures could arise from two potential scenarios. The first is that the functional group of the oleic acid is charged and acidic, thereby assisting in the hydrolysis and condensation of the silicic acid intermediate into condensed silica networks, while the glycerol head group of the monoolein structures creates energetically unfavorable interactions between the hydrophilic charged silicic acid intermediate. This is consistent with previous research on the condensation behavior of solubilized silica intermediates during sol-gel formation of porous structures with surfactants.[10] Additionally, oleic acid is less pure than monoolein

(90% rather than 99.999% as reported by manufacturers). This may mean that oleic acid structures are a mixture of OA and various fatty acids in addition to oxidized double bonds in the tail. This could potentially create a mixture more suitable for non-equilibrium assembly conditions and allow for mobility between phases before one phase fully condenses with the silica, which is less likely with a pure MO system. This is consistent with the method used, which has always shown the presence of multiple phases in our experiments.

In addition, this co-assembly method was also successfully applied to hexosome structures developed in the previous chapter. The method consistently showed hexagonal mesostructured ordering in TEM studies (Figure 3.2) and spiral lamellar cushioning frequently observed (Figure 3.3)

Fluorescence microscopy and PL data show successful loading of the dye Rhodamine B into the silica-lipid hybrid structures (Figure 3.4). Fluorescence could only be observed in powders that were spun out of solution, likely due to low signal to noise ratio when the sample is not concentrated. After changing the solution to 1x PBS buffer, no photoluminescence was observed, suggesting that an increase in salt concentration from pure water causes the Rhodamine B to unload from the sample. Successful loading of Rhodamine B demonstrated that this system may be of use to drug delivery and imaging. It would be extremely interesting to test if these samples could be loaded with materials that may have a more direct relevance to medical imaging. In particular, if these materials could be loaded with magnetic material or fabricated with a magnetic material rather than silica, they could be applied as a contrast agent in MRI techniques.

### 3.4 Conclusions

We have successfully developed several fabrication methods for mesoporous lipid-silica composites. These methods combine traditional sol-gel templating techniques with the field of lipid mesostructures to fabricate a composite material. Ordering is achieved in emulsion samples with OA showing the most consistent results, likely due to the acid head group aiding in the condensation of the silica precursor. Templated liquid crystal composites are achieved using the lipids MO and OA as well as using the block copolymer Pluronic ® F127.

We have also demonstrated that these materials may be loaded with hydrophobic materials, and that loading is sensitive to salt conditions (i.e. the load is released in saline solutions). This might open the door to using these materials in drug delivery as well as loading the material with magnetic components to use as contrast agents in medical imaging.

### 3.5 References

1. Prokesova, P.; Mintova, S.; Cejka, J.; Bein, T. Preparation of Nanosized Micro/MesoporousComposites Via Simultaneous Synthesis of Beta/MCM-48 Phases *Micro. Meso. Mater.* **2003,** *64* (1-3), 165-174

2. Cai, W.; Zhang, Y.; Jia, J.; Zhang, L. Semiconducting Optical Properties of Silver/Silica Mesoporous Composite *App. Phys. Lett.* **1998,** *73, 2709*

3. Wang, Z.l Liu, X.; Lv, M.; MEng, J. Simple Synthesis of Magnetic Mesoporous FeNi/Carbon Composites with a Large Capacity for the Immobilization of Biomolecules *Carbon* **2010,** *48* (11), 3182-3189

4. Slowing, I.I.; Trewyn, B.G.; Giri, S.; Lin, V.S.Y. Mesoporous Silica Nanoparticles for Drug Delivery Applications *Adv. Func. Mater.* **2007,** *17* (8), 1225-1236

5. Vallet-Regi, M.; Ramila, A.; del Real, R.P.; Perez-Pariente, J. A New Property of MCM-41: Drug Delivery System *Chem Mater.* **2001,** *13* (2), 308-311

6. Spicer, P.T. Progress in Liquid Crystalline Dispersions: Cubosomes. *Curr. Opin. Colloid Interface Sci.* **2005,** *10*, 274-279

7. Kaehr, B.; Townson, J.L.; Kalinich, R.M.; Awad, Y.H.; Swartzentruber, B.S.; Dunphy, D.R.; Brinker, C.J. Cellular Complexity Captured in Durable Silica Biocomposite *Proc. Natl. Acad. Sci. U.S.A.* **2012,** *109* (43), 17336-17341

8. Lakshmi, N.M.; Yalavarthi, P.R.; Vadlamudi, H.C.; Thanniru, J.; Yaga, G.K.H. Cubosomes as Targeted Drug Delivery Systems – A Biopharmaceutical Approach. *Curr. Drug Discovery Technol.***2014,** *11* (3), 181-188

9. Esposito, E.l Cortesi, R.; Drechsler, M.; Paccamiccio, L.; Mariani, P.; Contado, C.; Stellin, E.; Menegatti, E.; Bonina, F.; Puglia, C. Cubosome Dispersions as Delivery Systems for Percutaneous Administration of Indomethacin. *Pharmaceutical Research,* **2005,** *22* (12), 2163-2173

10. Van Opdenbosh, D.; Zollfrank, C. Cellulose-Based Biotemplated Silica Structuring. *Adv. Eng. Mater.* **2014,** *16* (6), 699-712

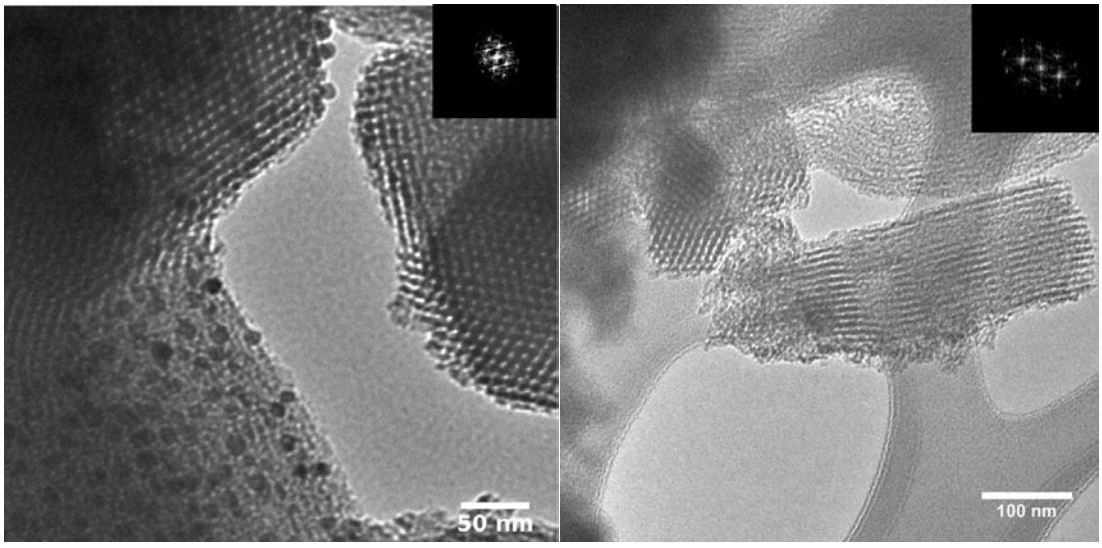


Figure 3.1 TEM micrographs of cubosome and liquid crystal structures. The image on the left shows the cubosome structure while the image on the right shows the liquid crystal structure. Insets are fast-fourier transforms showing the cubic symmetry.

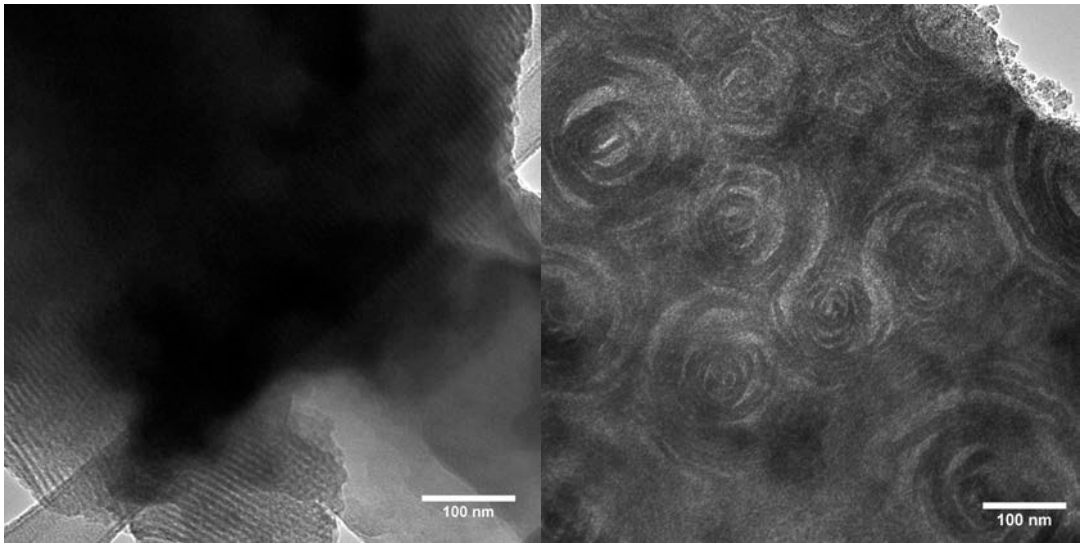


Figure 3.2 TEM micrographs of hexosome-silica composite structures. The image on the left clearly shows hexagonal ordering while the image on the right shows the spiral structure is reminiscent of the spiral lamellar cushioning found in many hexosome samples (see Figure 3.3).

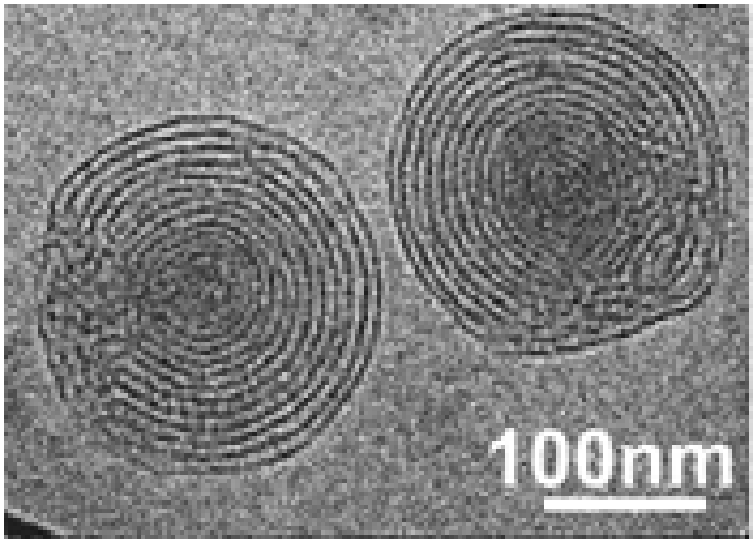


Figure 3.3 Cryo-TEM micrograph of hexosome samples made from phytantyl based surfactants, showing the spiral lamellar cushioning. Adapted from Fong, C. *et al. Soft Matt.* **2010,** *6,*4727-4741 with permission of The Royal Society of Chemistry.

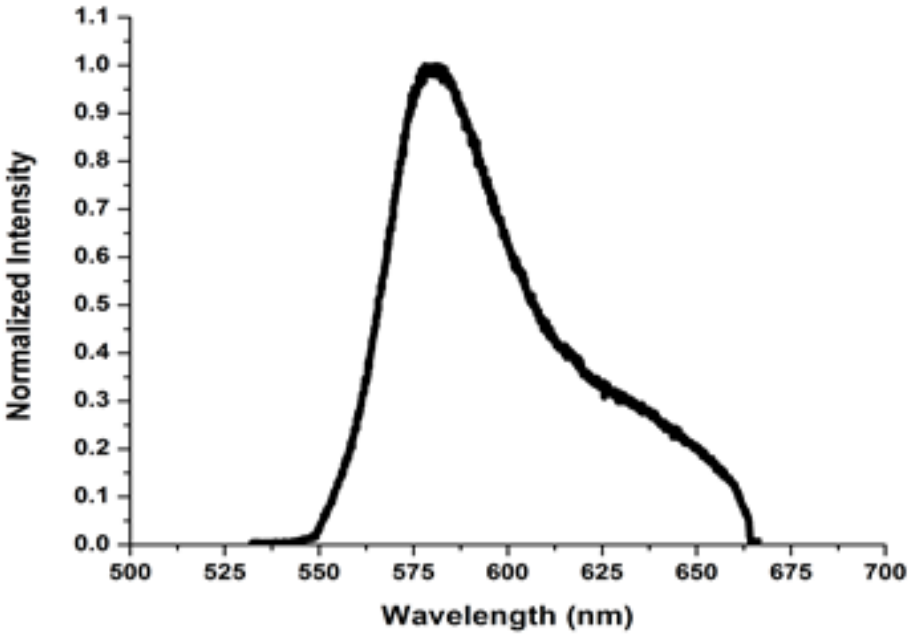


Figure 3.4 Photoluminescence spectrum of the Rhodamine B loaded oleic acid-silica cubosomes.

# CHAPTER 4

# SINTERED MESOPOROUS SILICA SOLIDS

## 4.1 Introduction

Silicon dioxide (silica) is a well-studied compound due to its chemical stability, well-known optical properties, and easy integration into existing materials. Mesoporous silica is one of the most common mesoporous materials investigated, and multiple fabrication methods have been developed[1] but supramolecular co-assembly has been the most common. A group at Mobil Corporation was the first to develop and patent a technique for synthesizing mesoporous silica (MCM-41), which uses basic sol-gel based techniques to template a lyotropic liquid crystal of small surfactant molecules.[2] Several years later, Galen Stucky's group at UCSB developed a self-assembly method based on acidic cooperative assembly of silica with surfactant molecules and larger polyethylene-oxide polypropylene-oxide block copolymers resulting in SBA-type mesoporous silica.[3]

The later method has been extensively used due to its versatility and tunability. Specifically, this method can be used to produce mesoporous structures with lamellar ordering, several hexagonal and cubic lattices, and

wormhole assemblies. Cubic lattice structures feature continuous silica frameworks while channel like two dimensional hexagonal lattices form from silica condensation around cylindrical micelles. All of these structures are based on a modification of the phase diagram of block copolymer-water systems.

Since the initial reports on silica mesostructured materials, extensive research has been done to extend synthesis into new compounds (metal-oxides, chalcogenides, metal, etc.) and macroscopic morphologies such as powders[1,3], monoliths[4] and thin-films.[5,6] Although this has produced excellent results and led to many applications in catalysis[7], sorption[8], sensing[9], optoelectronics[10], seperations[11], and drug delivery[12], there is a limit on the application of mesoporous materials: There is yet to be a suitable method for densification of these mesoporous materials into a bulk solid with tailored macroscopic shape and structure.

In this chapter, a powerful method for consolidating mesoporous silica powder into a solid disk shape (several millimeters thick and centimeters in diameter) will be described.[13] This method uses spark plasma sintering (SPS), a technique for densification of nanoparticles and porous powders without significantly altering the internal nanostructure of the materials.[14]

### 4.2 Methods

Mesoporous SBA-15 (2-D hexagonally ordered) silica powder was synthesized according to Zhao *et al.*. Briefly, 4 g of block copolymer Pluronic® P123 (donated by BASF) was dissolved in 120 mL of 2 M HCl (Sigma-Aldrich) and 30 mL of deionized water. To this solution, 8.5 g of TEOS (tetraethyl

orthosilicate, Sigma-Aldrich) was added and the solution was reacted for 20 hours at 37 °C followed by hydrothermal aging at 70 °C overnight. The sample was filtered and washed, followed by calcination at 500 °C for 3 hours with a 5 °C/min ramp rate. Mesoporous SBA-16 powder with a cubic mesostructural order was prepared as reported by Gobin[15]. Briefly, 3 g of the block copolymer Pluronic® F127 (donated by BASF) was dissolved in 144 mL deionized water and 13.8 mL 12.1 HCl. After stirring for 45 minutes at room temperature, 11 mL of butyl alcohol and 15.3 mL of TEOS was added to the mixture and the mixture was reacted for 24 hours at 45 °C followed by hydrothermal treatment at 70 °C overnight. Samples were washed, filtered, and calcined as described above.

SPS was performed by the Risbud group at the University of California, Davis, using their Sumitomo Dr. Sinter. Powders were placed in a die (typically graphite) and heated by passing a DC current through the die while a pressure was applied on the powder. For the mesoporous powders SPS was performed at a pressure of 10.6 MPa and temperatures between 600 and 1000 °C. Samples were sintered into solid disks with a diameter of 19 or 38 mm and a thickness of 3-5 mm.

The porosity and pore size of mesoporous silica samples before and after SPS consolidation were characterized by nitrogen adsorption/desorption measurements using Brunauer-Emmett-Teller theory (BET) and transition electron microscopy (TEM). BET was performed on a Micrometric TriStar II 3020 Surface Analysis instrument by nitrogen adsorption/desorption. TEM samples were prepared by grinding powders into a slurry with ethanol and depositing a

small drop onto 300 mesh copper grids with either continuous or lacey carbon/formvar coating. TEM studies were performed on a JEOL JEM-1400 Plus or FEI Technai 12 with 120 keV acceleration voltage, and on a JEOL 2800 at 200 keV acceleration voltage.

### 4.3 Results and Discussion

TEM studies illustrate preservation of the mesoporous ordering was preserved after SPS sintering at temperatures up to 950 °C (Figure 4.1). This is a somewhat surprising result, as higher temperatures would likely collapse the pores, but as the mechanism of SPS is Joule heating and electrical discharge between particle surfaces, it is likely that even at higher temperatures the inner regions of the particle are not subject to the higher temperature at the surface of the particle, thereby maintaining the mesostructural ordering inside the particles. While the surface area of the sintered samples shows the general trend of decreasing surface area with higher sintering temperatures (Table 4.1), it is noteworthy that at the lower sintering temperature of 600 °C the sample has only decreased the surface area by 18% of the unsintered powder. Surprisingly, even samples sintered at 900 °C possess a surface area of 217.7 ± 0.4 $m^2/g$.

Interestingly, at temperatures at or above 1000 °C the SPS process not only leads to complete collapse of porosity in the mesoporous samples but it also modifies the nature of silica. While silica is present in an amorphous phase in SPS sintered mesoporous samples below 1000 °C, above that temperature presence of cristobalite crystallites was observed in XRD and HR-TEM studies (Figure 4.2). We speculate this transformation is attributed to the unique SPS

process for which it is reasonable to assume that in an insulating sample charging builds up at the edges of the particle and leads to higher local temperature and pressure at the boundaries than in the bulk sample. This will lead locally to high enough temperatures to facilitate formation of cristobalite crystallites. At the same time, strain is created between the amorphous silica nanostructure and the ordered mesostructure due to an energetic preference for crystalline nanostructures at higher temperature and pressures, resulting in collapse of the mesoporous framework and full densification. Further experiments are underway to experimentally verify this proposed mechanism.

We have demonstrated that SPS is a suitable method for creating solid mesoporous materials while maintaining high surface area. This opens up the possibility of applying these materials to energy storage and electrochemical applications. For instance, by using either large pore or post-synthesis modified silica, there is the possibility of chemically modifying metal-oxides into carbides, metals, and using the metal-oxide structure as a template for porous carbon electrodes.

We have started to investigate how this may be done using two methods. Firstly, we used the magnesiothermal reduction method developed by the Sandhage group to convert silica into semiconducting silicon. Since this method reduces silica at low temperatures through the use of magnesium vapor,[16] we reasoned that this transformation should be possible with minimal damage to the mesoporous framework. Indeed, when applying this method to the sintered mesoporous silica disks, we observed in TEM studies both mesoporosity and the

appearance of lattice fringes, indicative of silicon crystallites (Figure 4.3). In addition, a strong increase in the sample conductance was observed, which also points to partly conversion of the insulating silica framework into semiconducting silicon.

Secondly, we investigated the possibility of converting the consolidated mesoporous silica disks into silicon carbide. For this, we infiltrated the porous network with sucrose solutions followed by pyrolysis[17] to create silica-carbon composites. The composite was then subjected to magnesium vapor to produce silicon carbide. XPS revealed a shift in the silicon 2p peak to 282 eV, a number consistent with silicon carbide (Figure 4.4). Although the results are preliminary, they are encouraging in suggesting that developing bulk mesoporous semiconductor or metal carbide materials is possible.

### 4.4 Conclusions

SPS has successfully been used for the consolidation of SBA-type mesoporous silica powder into a solid sample while maintaining the mesostructural ordering and open porosity. With this technique it was possible to fabricate discs of a variety of sizes, suggesting the possibility of tailored mesoporous shapes. At SPS temperatures above 1000 °C transformation of the porous amorphous silica framework into a nanocrystalline non-porous dense sample was observed. Furthermore, we have demonstrated first steps toward conversion of the mesoporous silica framework into silicon carbide and semiconducting silicon.

## 4.5 References

1. Rahmat, N.; Abdullah, A.Z.; Mohamed, A.R. A Review: Mesoporous Santa Barbara Amorphous-15 Types, Synthesis and Its' Applications Towards Biorefinery Production. *Am. J. Appl. Sci.* **2010,** *7* (10), 1579-1586

2. Kresge, C.T.; Leonowicz, M.E.; Roth, W.J.; Vartuli, J.C.; Beck, J.S. Ordered Mesoporous Molecular Sieves Synthesized by a Liquid-Crystal Template Mechanism. *Nature* **1992,** *359*, 710-712

3. Zhao, D.; Huo, Q.; Feng, J.; Chmelka, B.F.; Stucky, G.D. Nonionic Triblock and Star Diblock Copolymer and Oligomeric Surfactant Synthesis of Highly Ordered, Hydrothermally Stable Mesoporous Silica Structures. *J. Am. Chem. Soc.* **1998,** *120*, 6024-6036

4. Hu, Y.S.; Adelhelm, P.; Smaarsly, B.M.; Hore, S.; Antonietti, M; Maier, J. Synthesis of Hierachically Porous Ordered Carbon Monoliths with Highly Ordered Microstructure and Their Application in Rechargeable Lithium Batteries with High-Rate Capabilities. *Adv. Funct. Mater.* **2007,** *17* (12), 1873-1878.

5. Bartl, M.H.; Boettcher, S.W.; Hu, E.L.; Stucky, G.D. Dye-Activated Hybrid Organic/Inorganic Mesostructured Titania Waveguides. *J. Am. Chem. Soc.* **2004**, *126*, 10826-10827.

6. Zhao, D.; Yang, P.; Margolese, D.I.; Chmelka, B.F.; Stucky, G.D. Synthesis of Continuous Mesoporous Silica Thin-Films with Three-Dimensional Accessible Pore Structure. *Chem. Commun.* **1998,** *22*, 2499-2500

7. Taguchi, A.; Schuth, F. Ordered Mesoporous Materials in Catalysis. *Microporous Mesoporous Mater.* **2005,** *77* (1), 1-45

8. Pahalagedara, L.R.; Poyraz, A.S.; Song, W.; Kuo, C.H.; Pahalagedara, M.D.; Meng, Y.T.; Sulb, S.L. Low Temperature Desulfurization of $H_2S$: High Sorption Capacities by Mesoporous Cobalt Oxide via Increased $H_2S$ Diffusion *Chem. Mater.* **2014,** *26* (22), 6613-6621

9. Li, L.; He, S.; Liu, M.; Zhang, C.; Chen, W. Three-Dimensional Mesoporous Graphene Aerogel-Supported $SnO_2$ Nanocrystals for High-Performance $NO_2$ Gas Sensing at Low Temperature *Anal. Chem.* **2015,** *87* (3), 1638-1645

10. Crossland, E.J.W.; Noel, N.; Sivaram, M.; Leijtens, T.; Alexander-Weber, J.A.; Snaith, H.J. Mesoporous $TiO_2$ Single Crystals Delivering Enhanced Mobility and Optoelectronic Device Performance. *Nature* **2013,** *495*, 215-220

11. Zhao, J.; Gao, F.; Fu, Y.; Jin, W.; Yang, P.; Zhao, D. Biomolecule Seperation Using Large Pore Mesoporous SBA-15 as a Substrate in High Performance Liquid Chromatography *Chem. Commn.* **2002,** *7,* 752-753

12. Yang, P.; Gai, S.; Lin, J. Functionalized Mesoporous Silica Materials for Controlled Drug Delivery *Chem Soc. Rev.* **2012,** *41,* 3679-3698

13. Roehling, J.; Turner, B.A.; Benthem, K.; Risbud, S.; Bartl, M.H. Novel Materials from Sintered Mesoporous Silica. *In Preparation*

14. Risbud, S.H.; Han, Y.H. Preface and Historical Perspective on Spark Plasma Sintering. *Scr. Mater.* **2013,** *69* (2), 105-106

15. Gobin, O.C. SBA-16 Materials Synthesis, Diffusion and Sorption Properties. Ph.D. Dissertation, Laval University, Ste-Foy, Quebec, 2006.

16. Bao, Z.; Weatherspoon, M.R.; Shian, S.; Cai, Y.; Graham, P.D.; Allan, S.M.; Ahmad, G.; Dickerson, M.B.; Church, B.C.; Kang, Z.; Abernathy III, H.W.; Summers, C.J.; Liu, M.; Sandhage, K.H. Chemical Reduction of Three-Dimensional Silica Microassemblies Into Microporous Silicon Replicas. *Nature* **2007,** *446*, 172-175

17. Jun, S.; Joo, S.H.; Ryoo, R.; Kruk, M.; Jaroniec, M.; Liu, Z.; Ohsuna, T.; Terasaki, O. Synthesis of New, Nanoporous Carbon with Hexagonal Ordered Mesostructure. *J. Am. Chem. Soc.* **2000,** *122*, 10712-10713

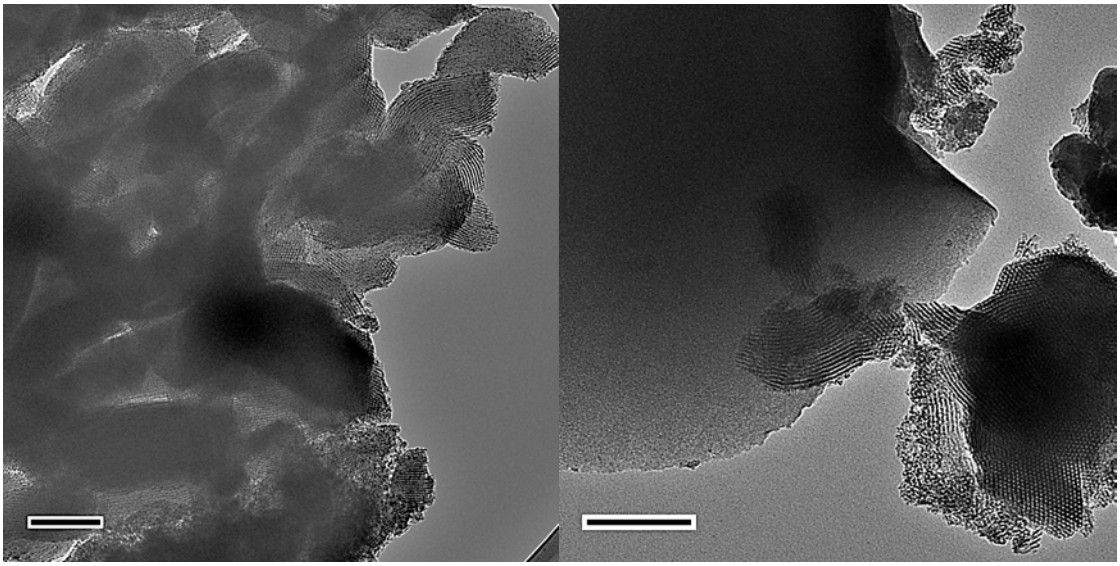

Figure 4.1 TEM micrographs showing sintered SBA-15 at 600 °C (left) and 850 °C (right). The image on the left shows the high degree of ordering remaining after sintering at a lower temperature while the image on the right shows the appearance of a disordered region. Scale bar in 200 nm.

Table 4.1 Table showing the various physical parameters of sintered SBA-15.

| **Temperature ($^{o}C$ )** | **Volume (mm3)** | **Density (g/cc)** | **Hardness ($kg/mm^2$)** | **Surface Area ($m^2/g$)** | **Average Pore Size (nm** |
|---|---|---|---|---|---|
| **600** | 2226.46 | 0.61 | 92.12 | 690.4 | 4.9 |
| **800** | 1794.77 | 0.75 | 188.16 | 485.5 | 5.0 |
| **850** | 1734.32 | 0.76 | 292.04 | 277.1 | 4.8 |
| **900** | 1779.24 | 0.80 | 248.92 | 254.1 | 4.8 |
| **950** | 1519.89 | 0.95 | N/A | 205.7 | 4.6 |
| **1000** | 1112.78 | 1.30 | 7151.06 | 178.9 | 4.6 |

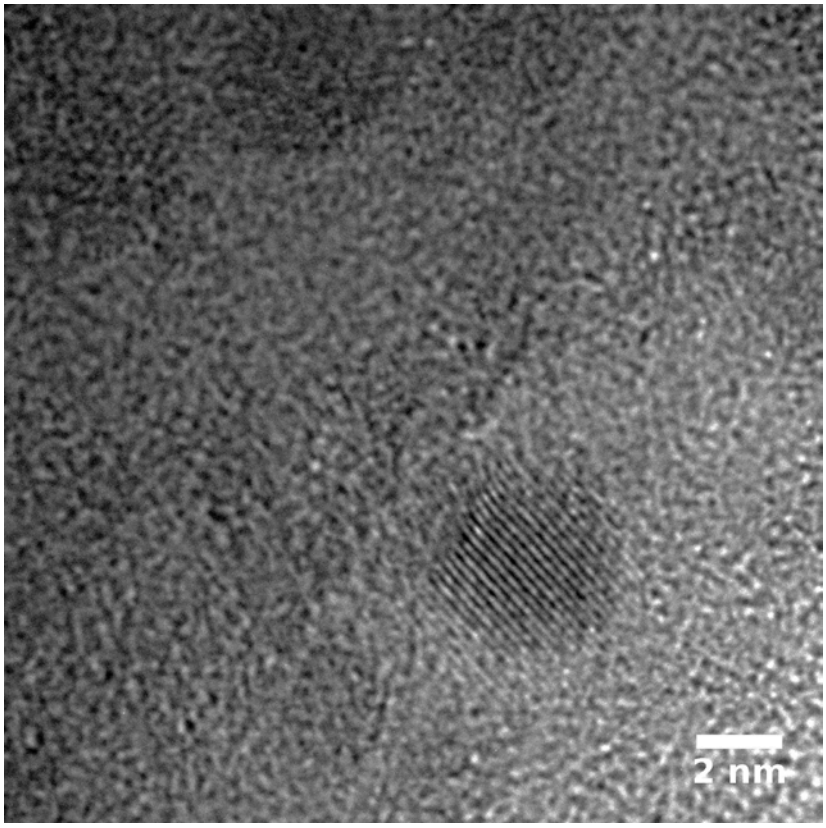


Figure 4.2 TEM micrograph showing the nanocrystallites formed under high temperature sintering.

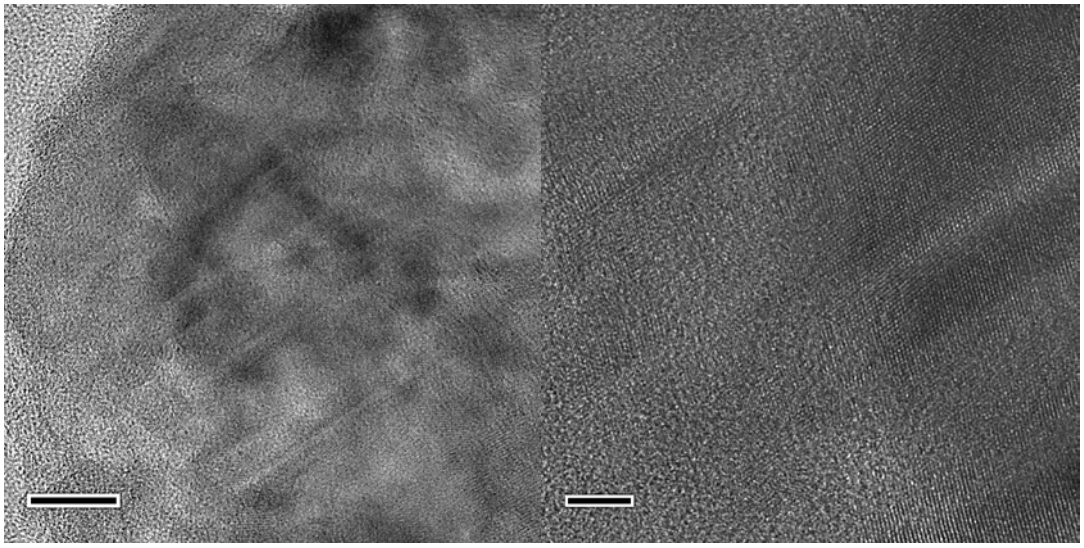

Figure 4.3 TEM micrograph showing the silicon lattice from the magnesiothermal reduction of mesoporous silica. The image on the left shows the porous silica while the image on the right is a high resolution image of the silicon lattice with scale bars 20 nm and 5nm, respectively.

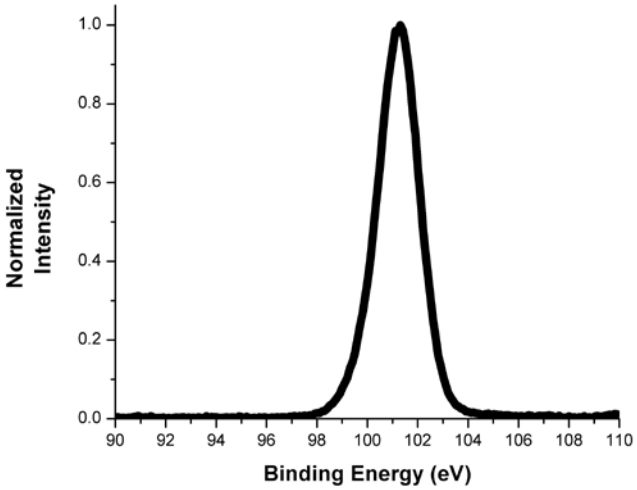


Figure 4.4 XPS spectrum showing the silicon 2p peak at 101.4227 ± 0.004 eV, a shift from the 104 eV peak typical for silicon dioxide and in good agreement with previously published data on silicon carbide.

# CHAPTER 5

# CONCLUSIONS AND OUTLOOK

Mesoporous and mesostructured materials have been developed and expanded to a well-defined field since the early discoveries of MCM and SBA silica.[1,2] Despite this explosion of techniques and applications, there is yet a definite link between mesoporous silica and the topologically similar phases of biological systems. This is surprising, as biological structures employ similar non-equilibrium assembly conditions and give rise to a myriad of unique applications.

This thesis has investigated and developed several novel techniques for mesostructured and mesoporous materials specifically looking at how biological systems can be employed to fabricate them. Monoolein cubosome mesostructures were successfully fabricated in high water concentrations and modified with the addition of a designer alpha helix peptide as confirmed by SAXS and cryo-TEM data. We also expanded this method to incorporate silica into the structure through a sol-gel based technique using low concentrations of a molecular silicate source in a weakly acidic solution. We also illustrated how spark plasma sintering can be applied to SBA-type silica for successful densification while maintaining a high surface area and mesostructure.

The first part of the thesis investigated lipid mesostructures and methods

for forming composite structures. Lipid structures were fabricated through a modified method from *Spicer et al.*[3,4] which creates cubosomes at high water content. By incorporating a designer alpha helix peptide into the structure, it was demonstrated how the phase behavior is changed dramatically at low concentrations, and the cubosome lattice constant is expanded at higher concentrations. Furthermore, transformation of the cubic lattice into a hexagonal structure was demonstrated. The hexagonal phase induced by the peptide showed remarkable thermal stability for lipid structures, which has not been observed in previous studies. Therefore, this study illustrates how there is a significant change in the phase behavior between the bulk phase and emulsified form of lipid mesostructures.

Composite structures were synthesized by incorporating silica with a low concentration of tetraethyl orthosilicate in a weakly acidic solution. This allowed for high degree of ordering despite multiple phases being present in the system. It was also observed that oleic acid leads to better ordering in the system compared to monoolein. This is likely due to the acidic functional group in the head of oleic acid. These structures were also capable of incorporating hydrophobic dyes and demonstrate fluorescence. The future application of these structures is quite varied. The successful loading of hydrophobic materials suggests possibilities in drug delivery by combining the chemical stability of silica with the bio-compatibility of the lipid component. These hybrid materials could also be developed for medical imaging applications, such as contrast agents through incorporation of magnetic or electron dense compounds.

We were also interested in whether this method could be applied to the block co-polymers used in traditional synthesis of mesoporous silica.[2] To investigate this, we used both the cubosome and lyotropic liquid crystal (LLC) method detailed in chapter 3 of this thesis. The LLC method gave a high degree of cubic ordering (Figure 5.1). This is not surprising, given the relatively wide region of the cubic phase in the Pluronic ® F127-water phase diagram.[5] In essence, this technique is similar to that developed for MCM-type materials except the mixing and condensation of the silica precursor is achieved by rapid freezing and heating instead of pressure.[1]

The cubosome method using Pluronic ® F127 produced a polydisperse sample that still exhibits a large amount of cubic ordering, as observed by TEM (Figure 5.1) The observed cubic structures from the Pluronic® F127 are intriguing, given the large difference in concentration (higher surfactant:TEOS ratio, lower surfactant:water ratio) compared to previously published methods.[2] To further investigate this method, we also tested the synthesis with and without sonication and the cubic symmetry was only observed when sonication was performed. The observation of ordering does lead to a question of the mechanism of assembly in dilute concentrations compared to traditional co-assembly methods. The sonication may input enough energy to overcome any kinetic barrier to assembly, which would explain the lack of cubic ordering without sonication. Verification of the kinetic theory could be done using two-dimensional nuclear magnetic resonance studies on samples at various stages of the assembly process to map the position the silicon atoms in relation to the block copolymer.

In addition to using block co-polymers, it would be value to expand the technique to produce composite structures directly into a defined shape to avoid the densification problem. To this end, we investigated fabrication of evaporative monolith structures by mixing 120 mL of 2 M HCl and 30 mL of deionized water with 113 µL or 1.125 mL of a monoolein solution of 10 mg/mL. After sufficient mixing time (approximately one hour), varying amounts of TEOS (4.5 to 18 mL) were added and mixed for several hours. After mixing, the sample was covered with a petri dish or in a centrifuge tube and placed into an oven at 50 °C for several days at a time. The monolith did gel into a distinct cylinder shape in the centrifuge tube when 18 mL of TEOS was used (Figure 5.2).While this wasn't a continuous structure, it does suggest this method could be optimized and used to produce monolith structures with similar properties to the cubosome composites.

Lastly, we have used spark plasma sintering to consolidate mesoporous silica into solid, hard disks without significant damage to the internal mesostructural pores and ordering. Lower sintering temperatures showed relatively minor changes in the surface area and ordering of SBA-15 mesoporous silica. Higher sintering temperatures showed the appearance of nanocrystallites of the cristobalite phase. Furthermore, proof-of-principle transformation reactions of the silica mesostructural framework were conducted, resulting in the formation of nanocrystalline silicon and silicon carbide structures. These initial steps demonstrate the potential of this approach for the fabrication of porous semiconductors.

The outlook for densified mesoporous material is extremely bright. The myriad of methods already developed can be easily applied and optimized for

densified systems, which offer a much greater ease of incorporation into existing systems. To name a few, this method could easily be applied to fabricate meosporous tungsten oxide, nickel, carbon, titanium carbide, zirconium, and titanium dioxide.

## 5.1 References

1. Kresge, C.T.; Leonowicz, M.E.; Roth, W.J.; Vartuli, J.C.; Beck, J.S. Ordered Mesoporous Molecular Sieves Synthesized by a Liquid-Crystal Template Mechanism. *Nature* **1992,** *359*, 710-712

2. Zhao, D.; Huo, Q.; Feng, J.; Chmelka, B.F.; Stucky, G.D. Nonionic Triblock and Star Diblock Copolymer and Oligomeric Surfactant Synthesis of Highly Ordered, Hydrothermally Stable Mesoporous Silica Structures. *J. Am. Chem. Soc.* **1998,** *120*, 6024-6036

3. Spicer, P.T. Progress in Liquid Crystalline Dispersions: Cubosomes. *Curr. Opin. Colloid Interface Sci.* **2005,** *10*, 274-279

4. Kaehr, B.; Townson, J.L.; Kalinich, R.M.; Awad, Y.H.; Swartzentruber, B.S.; Dunphy, D.R.; Brinker, C.J. Cellular Complexity Captured in Durable Silica Biocomposite *Proc. Natl. Acad. Sci. U.S.A.* **2012,** *109* (43), 17336-17341

5. Wanka, G.; Hoffman, H.; Ulbricht, W. Phase Diagrams and Aggregation Behavior of Poly(oxyethylene)-Poly(oxypropylene)-Poly(oxyethylene) Triblock Copolymers in Aqueous Solutions *Macromolecules* **1994,** *27*, 4145-4159

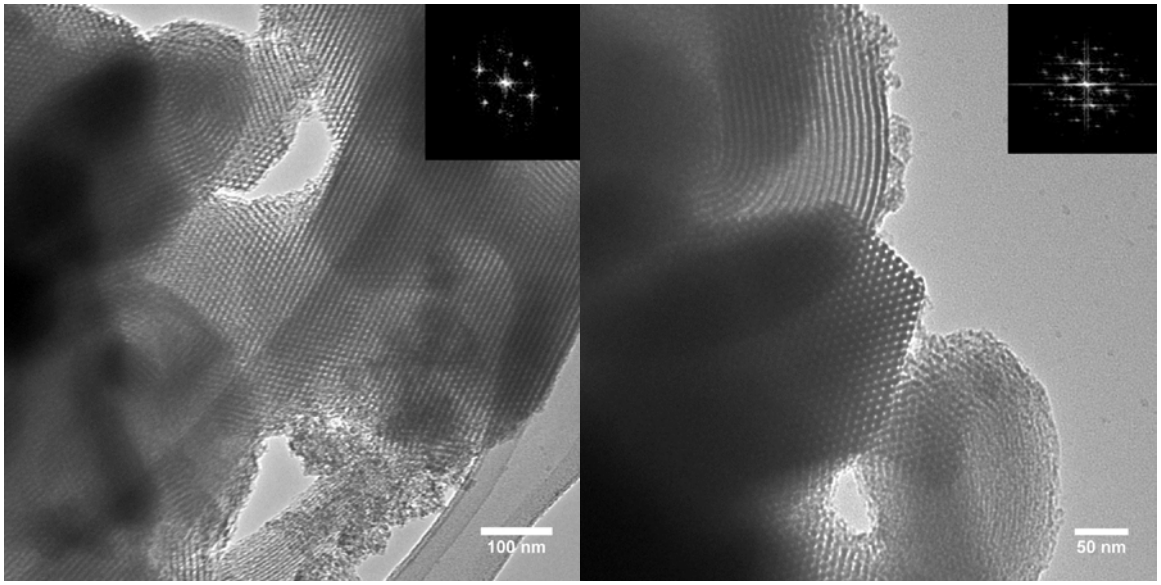


Figure 5.1 TEM micrograph showing the ordered cubic silica. The image on the left is from the liquid crystal method using Pluronic ® F127 while the image on the right is from the sonication method. Insets are the fast-Fourier transform.


Figure 5.2 Picture showing the evaporative monolith structure. The orange coloration is from degradation of the lipid during the evaporative assembly